PERIODICO di MINERALOGIA
established in 1930

DIPARTIMENTO
DI SCIENZE DELLA TERRA

SAPIENZA
UNIVERSITÀ DI ROMA

An International Journal of
Mineralogy, Crystallography, Geochemistry,
Ore Deposits, Petrology, Volcanology
and applied topics on Environment, Archaeometry and Cultural Heritage

Flow-through dissolution of mineral fibres under lysosomal conditions

Maria Cristina Di Carlo [1], Paolo Ballirano [1], Lorenzo Arrizza [1], Andrea Bloise [2], Maria Rita Montereali [3], Elisa Nardi [4], Fabrizio Bardelli [5], Alessandro Pacella[1,*]

[1] Department of Earth Sciences, Sapienza University of Rome, Piazzale Aldo Moro 5, I-00185, Rome, Italy
[2] Department of Biology, Ecology and Earth Sciences, University of Calabria, P. Bucci street, cubo 15b, 87036 Arcavacata di Rende, CS, Italy
[3] Italian National Agency for New Technologies, ENEA, Casaccia Research Centre, Via Anguillarese 301, I-00123 S. Maria di Galeria, Rome, Italy
[4] Institute for Environmental Protection and Research, ISPRA, via Vitaliano Brancati 48, 00144 Roma, Italy
[5] National Research Council, Institute of Nanotechnology (CNR-Nanotec), Rome, Italy

ARTICLE INFO

Submitted: December 2025
Accepted: April 2026
Available on line: April 2026

* Corresponding author:
alessandro.pacella@uniroma1.it

Doi: 10.13133/2239-1002/19219

How to cite this article:
Di Carlo M.C. et al. (2026)
Period. Mineral. 95, 169-177

ABSTRACT

Mineral fibre toxicity is widely considered to depend on their residence time in the lungs, and therefore on their biodurability. However, fibre dissolution is typically examined in closed batch systems, which evolve toward saturation and do not reproduce the continuous renewal of lung fluids. In this study, for the first time the dissolution behaviour of fibrous antigorite, chrysotile, and crocidolite was investigated in a flow-through system to better constrain their expected persistence *in vivo*. Flow-through experiments were conducted in simplified artificial lysosomal fluid (sALF) at pH 4.5 and 37 °C, with a flow rate of 0.047 mL min^{-1}. The concentrations of dissolved elements were determined by inductively coupled plasma optical emission spectroscopy (ICP-OES), while the incubated samples were analysed by powder X-ray diffraction (PXRD). Released Si was used to derive steady-state dissolution rates normalised to specific surface area. Fibrous antigorite and chrysotile show comparable Si-release rates of $1.03\pm0.02\cdot10^{-10}$ mol m^{-2} s^{-1} and $1.09\pm0.11\cdot10^{-10}$ mol m^{-2} s^{-1}, one order of magnitude higher than that of crocidolite ($1.22\pm0.06\cdot10^{-11}$ mol m^{-2} s^{-1}). When differences in specific surface area are considered, the biodurability of fibrous antigorite is only slightly lower than that of crocidolite, and therefore, both fibres are expected to persist significantly longer *in vivo* compared to chrysotile.

Keywords: Fibrous antigorite; asbestos; biodurability; flow-through dissolution; simulated lung fluids.

INTRODUCTION

The International Agency for Research on Cancer (IARC) classified asbestos as a Group 1 human carcinogen (IARC, 2012) in 1989 and subsequently great efforts have been made toward a global ban. Nonetheless, asbestos continues to represent one of the most critical occupational health challenges as several countries still largely employ it, particularly in Asia (IBAS, 2025; USGS, 2025). Worldwide, an estimated 125 million workers have been exposed in the workplace (Ramazzini, 2010), and asbestos-related diseases are responsible for approximately 250,000 deaths each year. This figure has even worsened in recent years (Furuya et al., 2018) and probably underestimates the true burden due to the

scarcity of epidemiological data from low- and middle-income countries where asbestos consumption has remained high (Han et al., 2023).

Asbestos includes chrysotile, a member of the serpentine subgroup, and five amphibole asbestos minerals: asbestos tremolite, asbestos actinolite, asbestos anthophyllite, asbestos grunerite (commercially known as amosite), and asbestos riebeckite (commercially known as crocidolite). Regulatory bans generally concern these minerals in industrial contexts, yet they do not extend to asbestos naturally occurring in rocks and soils that are not commercially exploited (NOA, naturally occurring asbestos), nor to elongated mineral particles (EMPs) without history of industrial use. Growing evidence of the potential hazard posed by EMPs has been reported by health and safety agencies (NIOSH, 2011), such as fibrous glaucophane and fibrous antigorite (Harper et al., 2008; Garabrant and Pastula, 2018; Gazzano et al., 2023). In this context, fibrous antigorite has recently attracted increasing attention, both because it is a polymorph of chrysotile and due to its widespread occurrence in serpentinite rocks and soils worldwide (Petriglieri et al., 2025 and references therein).

The toxicity of respirable mineral fibres results from a complex, multistep process governed by the interplay of their physical, chemical, and structural characteristics (Fubini and Mollo, 1995; Fubini and Areán, 1999; Donaldson et al., 2010; Bernstein et al., 2013). The biodurability of mineral fibres in lungs is recognised as a key factor in determining their pathogenic potential and refers to a material's resistance to chemical dissolution and degradation in the biological environment. Fibres with high biodurability are generally considered more toxic, as they can persist for long periods in the lungs and accumulate following chronic exposure (IARC, 2012; Gualtieri, 2018).

Dissolution rates of mineral fibres are usually inferred in simulated lung fluids by using closed-system batch reactors. Under these experimental conditions, the ions released during mineral dissolution progressively accumulate in the solution, whose composition evolves toward saturation, potentially inhibiting further fibre dissolution (Rozalén et al., 2017). Moreover, secondary phases often precipitate on the mineral surface making reactive sites no more accessible to fluids. Conversely, dissolution experiments performed in flow-through cells facilitate the measurement of the dissolution rate under fixed saturation state conditions (Brantley and Chen, 1995; Rozalén et al., 2008). When applied to biologically relevant fluids, these systems provide an experimental setting more representative of *in vivo* conditions, where fibre surfaces are continuously exposed to renewed fluids (Innes et al., 2021).

In this study, flow-through dissolution experiments were conducted for the first time on fibrous antigorite, chrysotile, and crocidolite fibres to provide a more accurate assessment of their biodurability in an acidic medium, representative of the macrophage lysosomal environment (pH 4.5). The concentrations of dissolved elements were determined by inductively coupled plasma optical emission spectroscopy (ICP-OES), while the incubated fibrous samples were analysed by powder X-ray diffraction (PXRD).

Materials

Flow-through experiments were carried out on fibrous samples of antigorite, crocidolite, and chrysotile. Sample information is reported in Table 1. The fibrous antigorite sample comes from veins within serpentinite bodies of the Gimigliano-Mount Reventino Unit, at San Mango d'Aquino (Calabria, Southern Italy) (Bloise et al., 2020).

Table 1. Summary of the mineral samples investigated. *Data from Pacella et al. (2019).

Mineral	Provenance	SSA (m^2g^{-1})	Crystal-chemical formula	Accessory phases
Fibrous antigorite	San Mango d'Aquino, Calabria (Italy)	4.0±0.5	$(Mg_{2.66}Fe^{2+}_{0.10}Fe^{3+}_{0.02}Al_{0.03}Mn_{0.01})_{\Sigma 2.82}(Si_{1.98}Al_{0.02})_{\Sigma 2.00}O_{5.00}(OH)_{3.67}$	No accessory phases
UICC Crocidolite	Koegas Mine (South Africa)	8.7±0.5	$^{A}Na_{0.03}{}^{B}Na_{2.00}{}^{C}(Fe^{2+}_{2.21}Fe^{3+}_{2.04}Mg_{0.75})_{\Sigma 5.00}{}^{T}(Si_{7.95}Al_{0.02})_{\Sigma 7.97}O_{22}{}^{O(3)}(OH)_2$	*Quartz [1.48±0.04 wt%], magnetite [1.85±0.06 wt%], calcite [1.30±0.09 wt%], siderite [1.12±0.09 wt%], minnesotaite [0.57±0.06 wt%]
UICC Chrysotile	Shabani Mine, Zvishavane (Zimbabwe)	27.0±0.5	$(Mg_{2.81}Fe^{2+}_{0.02}Fe^{3+}_{0.05}Al_{0.06})_{\Sigma 2.94}Si_{2.01}O_{5.00}(OH)_{4.00}$	Magnesite, pyroaurite, calcite, and dolomite

The sample has the following formula: $(Mg_{2.66}Fe^{2+}_{0.10}Fe^{3+}_{0.02}Al_{0.03}Mn_{0.01})_{\Sigma 2.82}(Si_{1.98}Al_{0.02})_{\Sigma 2.00}O_{5.00}(OH)_{3.67}$. The BET specific surface area SSA_{BET} is 4.0±0.5 $m^2\ g^{-1}$, and PXRD did not reveal the presence of accessory phases (Petriglieri et al., 2025). The crocidolite sample was provided by the Union International for Cancer Control (UICC) and comes from the Koegas Mine (South Africa). Its crystal-chemical formula is $^{A}Na_{0.03}{}^{B}Na_{2.00}{}^{C}(Fe^{2+}_{2.21}Fe^{3+}_{2.04}Mg_{0.75})_{\Sigma 5.00}{}^{T}(Si_{7.95}Al_{0.02})_{\Sigma 7.97}O_{22}{}^{O(3)}(OH)_2$ and ~6 wt.% of accessory phases were detected by PXRD (magnetite, quartz, calcite, siderite, and minnesotaite). The SSA_{BET} is 8.7±0.5 $m^2\ g^{-1}$ (Pacella et al., 2019, 2020). Chrysotile, also provided by the UICC, was collected from the Shabani asbestos mine in Zvishavane, Zimbabwe. Its chemical formula is $(Mg_{2.81}Fe^{2+}_{0.02}Fe^{3+}_{0.05}Al_{0.06})_{\Sigma 2.94}Si_{2.01}O_{5.00}(OH)_{4.00}$. This sample shows a particularly high specific surface area (SSA_{BET}=27.0±0.5 $m^2\ g^{-1}$). Accessory phases identified by PXRD include magnesite, pyroaurite, calcite, and dolomite.

Experimental

Experiments were performed using the set-up described in Rozalén et al. (2008). It consists of a system for solution circulation and allows a better understanding of the actual rate of fibre dissolution by simulating the continuous renewal of the physiological fluids within the lungs. A description of the components and their arrangement is provided below, with a schematic representation of the system shown in Figure 1.

The leaching solution is positioned upon a thermostatic magnetic stirrer to ensure the maintenance of a constant temperature of 37±1 °C and uniform mixing, with the aid of a magnetic bar. In preliminary experiments performed by using the standard ALF composition, the concentrations of dissolved elements resulted always below the analytical detection limit, most likely due to matrix interferences. For this reason, a simplified ALF solution (sALF) composed of sodium salts and citric acid as a chelating agent (Table 2) was used.

The sample is hosted in a 3D printed flow-through cell (Figure 2) composed of three compartments. Specifically, the fibres are in the central compartment confined in the lower part by a 5 µm nylon net filter and a 1.2 µm MF-Millipore™ MCE membrane (Merck Millipore, Ireland), and in the upper part by a 0.45 µm Durapore® PVDF membrane (Merck Millipore, Ireland). The solution enters the cell through the lower compartment and exits from the top of the cell. The total volume of the cell, i.e. the

Table 2. Composition of the simplified artificial lysosomal fluid used in flow-through dissolution experiments.

Compound	Concentration ($g\ L^{-1}$)
$C_6H_8O_7$ (citric acid)	20.8
NaOH (sodium hydroxide)	6.00
NaCl (sodium chloride)	3.21
Na_2SO_4 (sodium sulfate)	0.079
$C_6H_5Na_3O_7 \cdot 2H_2O$ (sodium citrate dihydrate)	0.077
pH	4.5

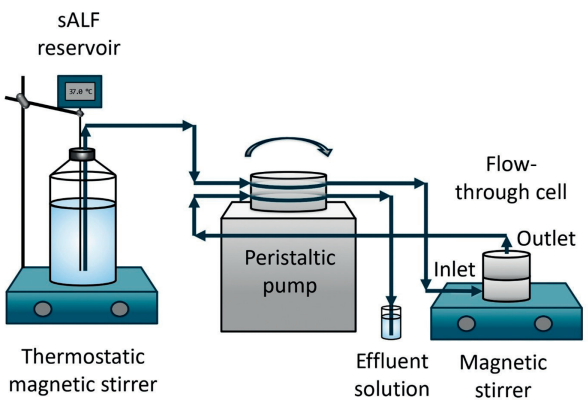

Figure 1. Schematic representation of the flow-through set-up, including peristaltic pump, thermostatic magnetic stirrer, and flow-through cell for solution circulation.

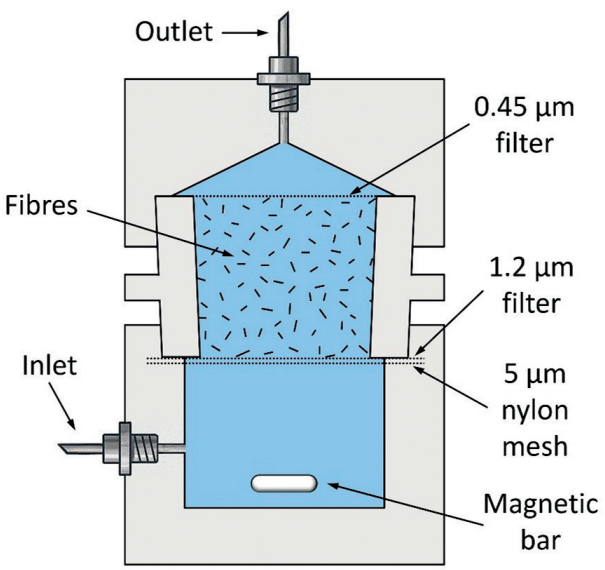

Figure 2. Schematic representation of the flow-through cell.

combined volume of the central compartment plus the upper- and lower-part sections, is 11.66 mL. The cell is positioned on a magnetic stirrer, with a magnetic bar placed at the bottom of the cell to continuously mix the solution and ensure homogeneity. A peristaltic pump (GILSON MINIPULS® 3) is used to drive the solution through the system, maintaining a steady flow set at 0.047±0.003 mL min^{-1}. This value is comparable with the human basal alveolar liquid clearance rate (~0.02 mL min^{-1}) reported by Sakuma et al. (1994). A tubing system connects the components and enables solution circulation. It consists of two tubing segments, one connecting the solution reservoir to the cell and the other connecting the cell to the collection vessel. Both segments are routed through the same peristaltic pump. PVC GILSON® tubing (inner diameter 0.25 mm) and BD INTRAMEDIC®, Clay Adams, polyethylene tubing (inner diameter 0.58 mm) were used. The effluent solutions are collected in Falcon tubes or larger LDPE bottles (VWR) for ICP-OES analysis.

Dissolution experiments were conducted in duplicate using approximately 100 mg of fibres, exactly weighed, for each test. They lasted up to 4 weeks for Calabrian fibrous antigorite and UICC chrysotile, and up to 2 weeks for UICC crocidolite, with samplings every 3 h on the first day and at longer intervals thereafter. The duration of the experiment was shorter for crocidolite since steady-state dissolution was reached earlier. The pH, checked at the end of each experiment, remained stable.

Methods

ICP on leaching solutions

The collected solutions were analysed by ICP-OES to quantify the cations released from the fibres. Measurements were performed using a Perkin Elmer Optima 2000 DV spectrometer (Perkin Elmer, USA) equipped with a cyclonic spray chamber. Before analysis, the samples were treated to break down the organic matrix of the sALF, which could cause interference in the measurement of the analytes of interest. Specifically, 5 mL of each solution were mixed with 2.5 mL of 67-69% HNO_3 traceSelect™ Ultra (Honeywell, Fluka, Canada) and 1 mL of 30% H_2O_2 Suprapur® (Meck KGaA, Germany) and then heated up to 100 °C using a DigiBlock mineralisation system (LabTech, Italy) for two h. At the end of the treatment, the digested samples were diluted to a final volume of 10 mL. Ca, Mg, Fe, SI and Al ICP standard solutions in nitric acid (Aristar, BDH) were used to prepare the calibration standard solutions for ICP-OES analysis. During analysis, the digested solutions were diluted 1:20, or 1:6 when necessary, with 1% nitric acid. Sodium release could not be quantified because its concentration in the solution exceeds the calibration range (0.05-10 mg L^{-1}). The accuracy of the measurements was monitored by periodically reanalysing the standard solutions.

Concentrations obtained by ICP-OES were processed to derive mean trends and associated variability. Because sampling times slightly differed between the two cells of each duplicate experiment, data were first linearly interpolated onto a common time grid. At each time point, the mean value was calculated as the arithmetic average of the two replicates, and variability was expressed as the sample standard deviation.

PXRD

PXRD analyses were carried out both before and after the dissolution experiments (4 weeks of sample incubation for fibrous antigorite and UICC chrysotile, and 2 weeks for UICC crocidolite). Diffraction patterns were collected with a Bruker AXS D8 Advance diffractometer (Bruker AXS, Karlsruhe, Germany) operating in θ/θ transmission geometry. The instrument was equipped with incident-beam focusing Göbel mirrors and a VÅntec-1 position-sensitive detector (PSD) fitted with radial soller slits. Samples were gently ground in an agate mortar under ethanol and mounted in borosilicate glass capillaries (0.4 mm in diameter). Data acquisition was performed using CuKα radiation over the 5-145° 2θ range, with a step size of 0.0218° 2θ and a counting time of 10 s per step.

RESULTS AND DISCUSSION

ICP-OES analysis of the digested solutions sampled from the leaching test for fibrous antigorite (Figure 3)

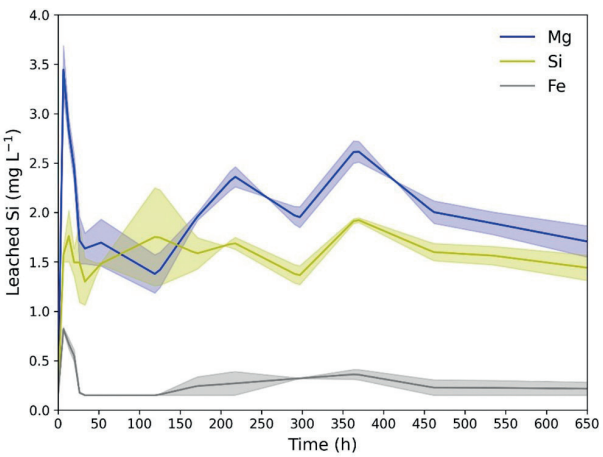

Figure 3 Concentration of leached cations (Mg, Si, Fe) during flow-through dissolution of Calabrian fibrous antigorite in sALF at pH 4.5, over 650 h of incubation. Lines represent the mean concentration of two replicate experiments after linear interpolation onto a common time grid. Shaded areas indicate ±1 standard deviation between replicates.

Table 3. Mineral phases identified by PXRD of in the investigated samples before and after flow-through dissolution in sALF. Percentages for the pristine UICC crocidolite sample are from Pacella et al. (2019).

Sample	Pristine	After incubation in sALF
Calabrian antigorite	Fibrous antigorite	Unaltered
UICC Crocidolite	Crocidolite [93.67± 0.19%], Quartz [1.48±0.04) wt%], Magnetite [1.85±0.06 wt%], Calcite [1.30± 0.09 wt%], Siderite [1.12± 0.09 wt%], Minnesotaite [0.57±0.06 wt%]	Unaltered
UICC Chrysotile	Chrysotile, Magnesite, Pyroaurite, Calcite, Dolomite	Chrysotile, Magnesite, Pyroaurite, Calcite, Dolomite, Magnetite, Talc, Quartz, Pentahydrite

showed for Mg an initial concentration peak during the first few h up to 3.5±0.4 mg L^{-1}. Subsequently, a decrease of Mg leaching with some fluctuations over time was observed. The initial rapid dissolution of silicates in flow-through experiments typically results from the dissolution of fine-grained material, strained grain surfaces, surfaces with structural defects (Rozalén et al., 2008 and references therein). Dissolution rate increases for fine-grained particles due to their very high surface-area-to-volume ratio and for strained grain surfaces, or surfaces with structural defects, because these are high-energy surface sites and thus thermodynamically less stable areas. Si release exhibited a more stable behaviour with respect to Mg, approaching steady-state (at concentrations of about 1.6±0.2 mg L^{-1}) already in the early stages of the dissolution process. Fe concentrations remained consistently very low, never exceeding 0.50 mg L^{-1} after the initial peak in the first h of sample incubation. For the fibrous antigorite sample, PXRD patterns collected before and after the experiment were completely overlapping indicating neither detectable structural changes nor formation of neo-precipitates (Table 3).

ICP-OES analysis of the solutions collected during the UICC crocidolite leaching experiment (Figure 4) showed that Fe was the most abundant cation released into solution. A pronounced peak in Fe concentration was detected within the first 24 h (8.6±1.0 mg L^{-1}), followed by an exponential decline up to 250 h that approaches to steady-state in the final stages of the experiment (0.39± 0.06 mg L^{-1}). The release of Fe is likely promoted by the chelating effect of citric acid present in sALF, which forms stable Fe-citrate complexes (Glusker, 1980). It's worth mentioning that flow-through dissolution experiments in modified Gamble's solutions have demonstrated that ligands such as citrate and oxalate can significantly influence the dissolution kinetics of amphiboles (Rozalén et al., 2013). Si displayed a similar behaviour, with an initial peak followed by a progressive decrease until steady-state is approached (at ca. 0.39±0.07 mg L^{-1}) with elapsed time (75 h). Mg release was observed only within the first 48 h of incubation, then starting to decline below the limit of quantification by 70 h of sample incubation. Similarly to the fibrous antigorite sample, PXRD patterns after 360 h of incubation, did not reveal neither mineral amorphization nor formation of neo-precipitates (Table 3).

ICP-OES analysis of the solutions sampled during the chrysotile sample dissolution experiment showed a significant Mg release during the first day up to 72±4 mg L^{-1} (Figure 5). Thereafter, its concentration undergoes a gradual decrease with elapsed time. Moreover, Si displays, after an initial peak within the first 8 h of

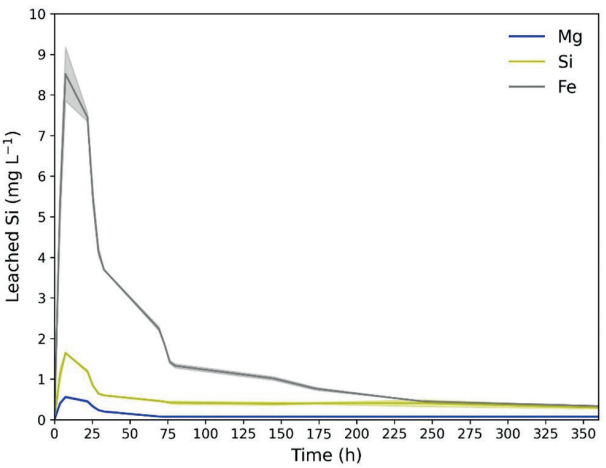

Figure 4. Concentration of leached cations (Mg, Si, Fe) during flow-through dissolution of UICC crocidolite in sALF at pH 4.5, over 360 h of incubation. Lines represent the mean concentration of two replicate experiments after linear interpolation onto a common time grid. Shaded areas indicate ±1 standard deviation between replicates.

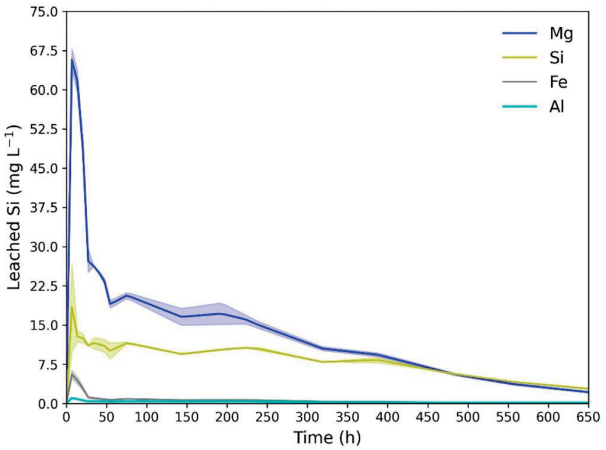

Figure 5. Concentration of leached cations (Mg, Si, Fe, Al) during flow-through dissolution of UICC chrysotile in sALF at pH 4.5, over 650 h of incubation. Lines represent the mean concentration of two replicate experiments after linear interpolation onto a common time grid. Shaded areas indicate ±1 standard deviation between replicates.

sample incubation, a steady-state release (ca. 11.3±1.1 mg L^{-1}) up to approximately 300 h from the beginning of the experiment. Later, a progressive decline in Si concentration is observed. The preferential leaching of Mg with respect to Si is consistent with the faster dissolution of the octahedral layers in the serpentine structure at acidic pH, followed by the slower dissolution of the tetrahedral silicate layers (Rozalén et al., 2014; Lacinska et al., 2016; Zhao et al., 2024). Moreover, the progressive decline in Si concentration observed after ca. 300 h is likely related to the dissolution of a significant portion of chrysotile fibres over time. The loss of chrysotile fibres following incubation in sALF was evident by visual observation of the recovered sample at the end of the experiment (4 weeks). Accordingly, PXRD evidenced in the leached sample a relative enrichment of accessory phases (magnetite, talc and quartz) as compared to the pristine sample. PXRD pattern revealed no significant evidence of loss of fibre crystallinity (Figure 6) albeit the increase of the intensity of the broad band centred at ca. 22°2θ, caused by the glass of the capillary, seems to suggest the occurrence of some amorphous material. PXRD also identified minor amounts of pentahydrite (Mg-sulphate) after dissolution (Table 3), presumably resulting from precipitation processes promoted by the high Mg release from the fibres into the solution.

Dissolution rates of the fibrous samples investigated under flow-through conditions were compared using Si concentrations in the effluent solutions at steady state, after normalization to mineral surface area. Si is generally the rate-determining element in silicate dissolution (Oze and Solt, 2010), and therefore, it was used for rate calculation. Results obtained highlighted that the fibrous antigorite and chrysotile have comparable dissolution rates under acidic conditions, significantly higher than that of UICC crocidolite (Figure 7). This result is consistent with the well-established contrast between chrysotile and amphibole asbestos in both *in vitro* and *in vivo* studies, with chrysotile exhibiting lower biodurability and rapid

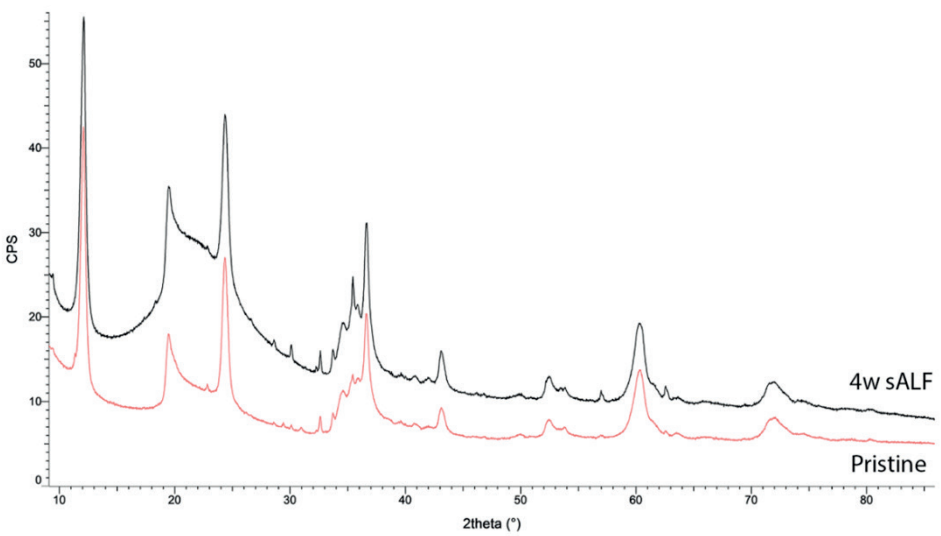

Figure 6. Experimental PXRD patterns of pristine UICC chrysotile (red) and the sample after 4 weeks of incubation in sALF (black). Spectra have been vertically displaced for clarity. The small plateau at the onset of the diffraction patterns is caused by partial obstruction of the incident beam by the knife-edge of the focussing mirrors.

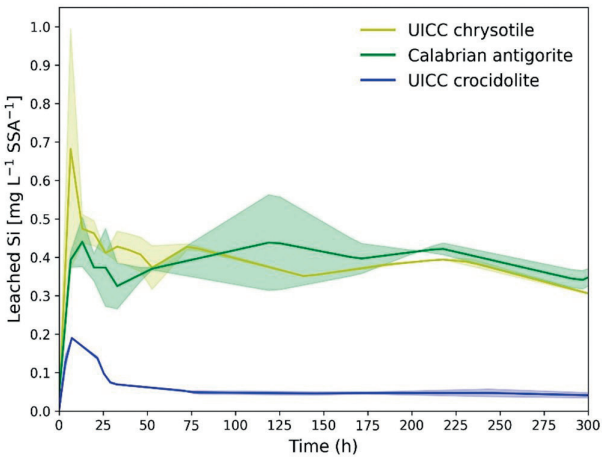

Figure 7 Flow-through dissolution experiments in sALF (pH 4.5). Normalized Si release (mg L^{-1} per SSA) for the same samples, over the same time interval. Lines represent the mean concentration of two replicate experiments after linear interpolation onto a common time grid. Shaded areas indicate ±1 standard deviation between replicates.

clearance from the lungs (Bernstein et al., 2005a, 2005b, 2004; Bernstein and Hoskins, 2006).

CONCLUSIONS

In this work the biodurability of fibrous antigorite, chrysotile and crocidolite fibres was investigated in sALF at pH 4.5 using a flow-through cell (open system), to mimic the interaction between fibres and macrophages during phagocytosis. It must be pointed out that the open system allowed us to replicate fluid replenishment occurring *in vivo* conditions. Si release rates, calculated as:

$$r_{si} = \overline{C}_{si} \cdot \frac{Q}{SSA \cdot M}$$

where $\overline{C}_{si}$ the average Si concentration at steady state (mol L^{-1}), Q is the flow rate (L s^{-1}), SSA the specific surface area (m^2 g^{-1}), and M the mass (g), highlighted that the dissolution rate of fibrous antigorite and chrysotile under acidic conditions is comparable ($1.03\pm0.02\cdot10^{-10}$ mol m^{-2} s^{-1} and $1.09\pm0.11\cdot10^{-10}$ mol m^{-2} s^{-1}, respectively), and about one order of magnitude higher than that of UICC crocidolite ($1.22\pm0.06\cdot10^{-11}$ mol m^{-2} s^{-1}). The Si-based dissolution rate measured here for chrysotile agrees with *in vivo* evidence of rapid pulmonary clearance and limited biodurability of chrysotile compared with that of amphibole asbestos (Bernstein et al., 2005a, 2005b, 2004, 2003; Hesterberg et al., 1998, 1996). Moreover, for fibres 5-20 µm in length, reported half-times are 0.3-29.7 days for chrysotile versus 262 days for crocidolite (Bernstein and Hoskins, 2006).

Notably, although fibrous antigorite exhibits a dissolution rate comparable to that of its polymorph chrysotile, antigorite fibres are expected to persist much longer *in vivo* owing to their smaller specific surface area.

ACKNOWLEDGEMENTS

This study was carried out within the RETURN Extended Partnership and received funding from the European Union Next-Generation EU (National Recovery and Resilience Plan - NRRP, Mission 4, Component 2, Investment 1.3 - D.D. 1243 2/8/2022, PE0000005).

REFERENCES

Bernstein D., Dunnigan J., Hesterberg T., Brown R., Velasco J.A.L., Barrera R., Hoskins J., Gibbs A., 2013. Health risk of chrysotile revisited. Critical Reviews in Toxicology 43, 154-183.

Bernstein D.M. and Hoskins J.A., 2006. The health effects of chrysotile: Current perspective based upon recent data. Regulatory Toxicology and Pharmacology 45, 252-264.

Bernstein D., Chevalier J., Smith P., 2005a. Comparison of Calidria Chrysotile Asbestos to Pure Tremolite: Final Results of the Inhalation Biopersistence and Histopathology Examination Following Short-Term Exposure. Inhalation Toxicology 17, 427-449.

Bernstein D., Rogers R., Smith P., 2005b. The biopersistence of Canadian chrysotile asbestos following inhalation: final results through 1 year after cessation of exposure. Inhalation Toxicology 17, 1-14.

Bernstein D.M., Rogers R., Smith P., 2004. The Biopersistence of Brazilian Chrysotile Asbestos Following Inhalation. Inhalation Toxicology 16, 745-761.

Bernstein D.M., Chevalier J., Smith P., 2003. Comparison of Calidria Chrysotile Asbestos to Pure Tremolite: Inhalation Biopersistence and Histopathology Following Short-Term Exposure. Inhalation Toxicology 15, 1387-1419

Bloise A., Ricchiuti C., Punturo R., Pereira D., 2020. Potentially toxic elements (PTEs) associated with asbestos chrysotile, tremolite and actinolite in the Calabria region (Italy). Chemical Geology 558, 119896.

Brantley S.L. and Chen Y., 1995. Chemical weathering rates of pyroxenes and amphiboles, in: White A.F., Brantley Susan L., Chemical Weathering Rates of Silicate Minerals. De Gruyter, 119-172.

Donaldson K., Murphy F.A., Duffin R., Poland C.A., 2010. Asbestos, carbon nanotubes and the pleural mesothelium: a review of the hypothesis regarding the role of long fibre retention in the parietal pleura, inflammation and mesothelioma. Particle and Fibre Toxicology 7, 5.

Fubini B. and Areán C.O., 1999. Chemical aspects of the toxicity of inhaled mineral dusts. Chemical Society Reviews 28, 373-381.

Fubini B. and Mollo L., 1995. Role of iron in the reactivity of mineral fibers. Toxicology Letters 82-83, 951-960.

Furuya S., Chimed-Ochir O., Takahashi K., David A., Takala J., 2018. Global Asbestos Disaster. International Journal of Environmental Research and Public Health 15, 1000.

Garabrant D.H. and Pastula S.T., 2018. A comparison of asbestos fiber potency and elongate mineral particle (EMP) potency for mesothelioma in humans. Toxicology and Applied Pharmacology, The Monticello Conference on Elongated Mineral Particles 361, 127-136.

Gazzano E., Petriglieri J.R., Aldieri E., Fubini B., Laporte-Magoni C., Pavan C., Tomatis M., Turci F., 2023. Cytotoxicity of fibrous antigorite from New Caledonia. Environmental Research, The Monticello II Conference on Elongate Mineral Particles 230, 115046.

Glusker J.P., 1980. Citrate conformation and chelation: enzymic implications. Accounts of Chemical Research 13, 345-352.

Gualtieri A.F., 2018. Towards a quantitative model to predict the toxicity/pathogenicity potential of mineral fibers. Toxicology and Applied Pharmacology 361, 89-98.

Han J., Park S., Yon D.K., Lee S.W., Woo W., Dragioti E., Koyanagi A., Jacob L., Kostev K., Radua J., Lee S., Shin J.I., Smith L., 2023. Global, Regional, and National Burden of Mesothelioma 1990-2019: A Systematic Analysis of the Global Burden of Disease Study 2019. Annals of the American Thoracic Society 20, 976-983.

Harper M., Lee E.G., Doorn S.S., Hammond O., 2008. Differentiating Non-Asbestiform Amphibole and Amphibole Asbestos by Size Characteristics. Journal of Occupational and Environmental Hygiene 5, 761-770.

Hesterberg T.W., Chase G., Axten C., Miller W.C., Musselman R.P., Kamstrup O., Hadley J., Morscheidt C., Bernstein D.M., Thevenaz P., 1998. Biopersistence of Synthetic Vitreous Fibers and Amosite Asbestos in the Rat Lung Following Inhalation. Toxicology and Applied Pharmacology 151, 262-275.

Hesterberg T.W., Miiller W.C., Musselman R.P., Kamstrup O., Hamilton R.D., Thevenaz P., 1996. Biopersistence of Man-Made Vitreous Fibers and Crocidolite Asbestos in the Rat Lung Following Inhalation. Fundamental and Applied Toxicology 29, 267-279.

IARC, 2012. Arsenic, metals, fibres, and dusts. IARC Monographs on the evaluation of Carcinogenic Risks to Humans 100, 11-465.

Innes E., Yiu H.H.P., McLean P., Brown W., Boyles M., 2021. Simulated biological fluids - a systematic review of their biological relevance and use in relation to inhalation toxicology of particles and fibres. Critical Reviews in Toxicology 51, 217-248.

International Ban Asbestos Secretariat (IBAS), 2025. Current situation worldwide: Countries with asbestos bans and restrictions [WWW Document]. URL https://www.ibasecretariat.org (accessed 8.12.25).

Lacinska A.M., Styles M.T., Bateman K., Wagner D., Hall M.R., Gowing C., Brown P.D., 2016. Acid-dissolution of antigorite, chrysotile and lizardite for *ex situ* carbon capture and storage by mineralisation. Chemical Geology 437, 153-169.

National Institute for Occupational Safety and Health (NIOSH), 2011. Current intelligence bulletin 62: asbestos fibers and other elongate mineral particles: state of the science and roadmap for research. (DHHS (NIOSH) Publication No. 2011-159). U.S. Department of Health and Human Services, Centers for Disease Control and Prevention, Cincinnati, OH.

Oze C., Solt K., 2010. Biodurability of chrysotile and tremolite asbestos in simulated lung and gastric fluids. American Mineralogist 95, 825-831.

Pacella A., Andreozzi G., Nodari L., Ballirano P., 2019. Chemical and structural characterization of UICC crocidolite fibres from Koegas Mine, Northern Cape (South Africa).

Pacella A., Tomatis M., Viti C., Bloise A., Arrizza L., Ballirano P., Turci F., 2020. Thermal inertization of amphibole asbestos modulates Fe topochemistry and surface reactivity. Journal of Hazardous Materials 398, 123119.

Petriglieri J.R., Capitani G., Ballirano P., Barale L., Piana F., Tomatis M., Di Carlo M.C., Gianchiglia F., Campopiano A., Olori A., Bruno M.R., Montereali M.R., Nardi E., Fantauzzi M., Rossi A., Skogby H., Belluso E., Turci F., Pacella A., 2025. Naturally occurring asbestos in Southern Italy: Geological and mineralogical investigation of fibrous antigorite from Calabrian serpentinites in view of its hazard assessment. Science of The Total Environment 970, 178970.

Ramazzini C., 2010. Asbestos Is Still With Us: Repeat Call for a Universal Ban. Archives of Environmental & Occupational Health 65, 121-126.

Rozalén M., Huertas F.J., Pacella A., Ballirano P., 2017. Dissolution and biodurability of mineral fibres. In: A.F. Gualtieri (Ed.) "Mineral fibres: crystal chemistry, chemical-physical properties, biological interaction and toxicity". European Mineralogical Union, London, 17-64.

Rozalén M., Huertas F.J., Brady P.V., Cama J., García-Palma S., Linares J., 2008. Experimental study of the effect of pH on the kinetics of montmorillonite dissolution at 25 °C. Geochimica et Cosmochimica Acta 72, 4224-4253.

Rozalén M., Ramos M.E., Fiore S., Gervilla F., Huertas F.J., 2014. Effect of oxalate and pH on chrysotile dissolution at 25 °C: An experimental study. American Mineralogist 99, 589-600.

Rozalén M., Ramos M.E., Huertas F.J., Fiore S., Gervilla F., 2013. Dissolution kinetics and biodurability of tremolite particles in mimicked lung fluids: Effect of citrate and oxalate. Journal of Asian Earth Sciences 77, 318-326.

Sakuma T., Okaniwa G., Nakada T., Nishimura T., Fujimura S., Matthay M.A., 1994. Alveolar fluid clearance in the resected human lung. American journal of respiratory and critical care medicine, 150, 305-10.

U.S. Geological Survey (USGS), 2025. Mineral Commodity

Summaries 2025: Asbestos. U.S. Department of the Interior.
Zhao D., Sun H., Peng T., Zeng L., 2024. Ionic dissolution and structural evolution of chrysotile and lizardite at the mineral-water interface: reactions in sulfuric acid solution. Clays and Clay Minerals 72, e32.

This work is licensed under a Creative Commons Attribution 4.0 International License CC BY-NC-SA 4.0.